The Planetary Science Journal, 5:67 (10pp), 2024 March https://doi.org/10.3847/PSJ/ad226d

Fermi Resonance and the Quantum Mechanical Basis of Global Warming

R. Wordsworth[1,2], J. T. Seeley[1], and K. P. Shine[3]
[1] School of Engineering and Applied Sciences, Harvard University, Cambridge, MA 02138, USA; rwordsworth@seas.harvard.edu
[2] Department of Earth and Planetary Sciences, Harvard University, Cambridge, MA 02138, USA
[3] Department of Meteorology, University of Reading, Reading, RG6 6ET, UK
Received 2023 July 14; revised 2024 January 16; accepted 2024 January 17; published 2024 March 11

Abstract

Although the scientific principles of anthropogenic climate change are well-established, existing calculations of the warming effect of carbon dioxide rely on spectral absorption databases, which obscures the physical foundations of the climate problem. Here, we show how CO_2 radiative forcing can be expressed via a first-principles description of the molecule's key vibrational-rotational transitions. Our analysis elucidates the dependence of carbon dioxide's effectiveness as a greenhouse gas on the Fermi resonance between the symmetric stretch mode ν_1 and bending mode ν_2. It is remarkable that an apparently accidental quantum resonance in an otherwise ordinary three-atom molecule has had such a large impact on our planet's climate over geologic time, and will also help determine its future warming due to human activity. In addition to providing a simple explanation of CO_2 radiative forcing on Earth, our results may have implications for understanding radiation and climate on other planets.

Unified Astronomy Thesaurus concepts: Earth atmosphere (437); Greenhouse effect (2314); Planetary atmospheres (1244); Planetary climates (2184)

1. Introduction

Carbon dioxide is an essential greenhouse gas on all rocky planets in the solar system with significant atmospheres (Venus, Earth, and Mars). On Earth, the carbonate-silicate cycle regulates atmospheric CO_2 on geological timescales, but the last 150 yr has seen a rapid rise in concentrations from approximately 280 ppmv to 415 ppmv (Tziperman 2022), due to burning of fossil fuels by humans and land use changes (Friedlingstein et al. 2022). Earth's global-mean surface temperature has risen by approximately 1 K during this same period, with most of the warming a direct result of this CO_2 increase. CO_2 affects surface temperature because it is a greenhouse gas: It absorbs more effectively at thermal infrared frequencies than the near-infrared and visible frequencies where solar radiation peaks. As a result, increasing levels of atmospheric CO_2 shifts the emission of thermal radiation to space to higher-altitude regions of the atmosphere, where air is less dense and colder. This colder air releases less thermal radiation, so increasing CO_2 decreases total emission to space for fixed surface and atmospheric temperatures. The magnitude of this decrease is defined as the radiative forcing of CO_2.

Atmospheric mixing is fast compared to the rate of CO_2 emission and removal, so to a first approximation the CO_2 concentration is uniform in Earth's lower atmosphere. The stratosphere-adjusted radiative forcing due to an increase in the atmospheric CO_2 molar concentration from x_0 to x is typically expressed as[4]

$$\Delta F \approx +\alpha \ln[x/x_0], \tag{1}$$

where α is defined as the CO_2 radiative forcing parameter. Global-mean calculations from detailed radiative transfer codes using tabulated spectroscopic data yield $\alpha \approx 5.35\ \mathrm{W\,m^{-2}}$ (Myhre et al. 1998), with an estimated accuracy of around 10%. Once the atmosphere and ocean have thermally equilibrated, this radiative forcing gives rise to a surface-temperature change of magnitude

$$\Delta T_s \approx +\lambda^{-1}\Delta F, \tag{2}$$

where the parameter λ is the climate feedback parameter, with units of $\mathrm{W\,m^{-2}\,K^{-1}}$. Based on data from a range of observational and modeling sources, the sixth assessment report of the Intergovernmental Panel on Climate Change (IPCC AR6) stated that ΔT_s for a doubling of CO_2 is "very likely" (i.e., with greater than 90% probability) in the range 2 to 5 K, with a best estimate of 3 K (Masson-Delmotte et al. 2021). Since the radiative forcing for CO_2 doubling $\Delta F_{2\times} = 5.35 \ln(2) = 3.71\ \mathrm{W\,m^{-2}}$, this indicates a value of between 0.74 and $1.85\ \mathrm{W\,m^{-2}\,K^{-1}}$ for λ.

Given the clear correspondence between observations and the results of sophisticated climate models, the scientific basis of climate change is indisputable. In addition, many comprehensive descriptions of the physics of climate and global warming, including the specifics of the radiative effects of CO_2 doubling, already exist (Pierrehumbert 2011; Wilson & Gea-Banacloche 2012; Zhong & Haigh 2013; Mlynczak et al. 2016; Dufresne et al. 2020; Jeevanjee et al. 2021; Romps et al. 2022; Tziperman 2022; Shine & Perry 2023). Despite this, it is currently still not possible to derive Equation (1) directly starting from fundamental properties of the CO_2 molecule. This is an important objective, because analytic methods are a powerful tool to increase understanding and elucidate the results of numerical simulations. Here, we build on previous efforts and show how this can be achieved, via a synthesis of molecular spectroscopy and climate physics. Our analysis here focuses on Earth's present-day climate, but potential applications to other planets in the solar system and exoplanets are discussed in Section 6.

[4] This differs slightly from the effective radiative forcing definition now used by the IPCC (Masson-Delmotte et al. 2021), although the difference is not important for our purposes. See also discussion in Section 5.

2. A Simple Empirical Model of CO_2 Radiative Forcing

In several recent papers (Wilson & Gea-Banacloche 2012; Jeevanjee et al. 2021; Romps et al. 2022), it has been shown that key features of CO_2 radiative forcing can be captured using a simplified representation of atmospheric radiative transfer combined with an empirical approach to CO_2 spectroscopy. Absorption by CO_2 in the thermal infrared at Earth-like concentrations is dominated by a broad collection of bands centered around 20 THz (667 cm^{-1} in wavenumber units)[5] that has a "triangular" shape in logarithmic units (Figure 2). Because of this, this collection of bands can approximately be represented using the formula

$$\ln[\sigma/\sigma_{\rm cen}] = -\frac{|\nu - \nu_{\rm cen}|}{w}, \quad (3)$$

for absorption cross section σ. Here, $\sigma_{\rm cen}$ is the value of σ at the band center, ν is the frequency, $\nu_{\rm cen}$ is the frequency of the band center, and w is a band structure coefficient, such that a smaller value of w leads to a narrower band. Numerical estimation of w from HITRAN spectroscopic data or line-by-line spectral radiative forcing calculations yields a value of around 0.37 THz (12.5 cm^{-1}), with the value somewhat dependent on the fitting approach chosen (Jeevanjee et al. 2021; Romps et al. 2022).

Taking the angle-averaged optical depth τ as increasing downwards from the top of the atmosphere to the surface, we can write a small change in τ as

$$d\tau = \frac{x\sigma}{\overline{\mu} m_a}\frac{dp}{g}, \quad (4)$$

where $\overline{\mu}$ is the mean propagation angle of upwelling infrared photons, p is pressure, g is gravity, and m_a is the mean molecular mass of air. If we assume a linear dependence of σ on pressure due to line broadening such that $\sigma = \sigma_0(p/p_0)$, where p_0 is a reference pressure (Table 1), then[6]

$$\tau = \frac{x\sigma_0 p^2}{2g\overline{\mu} m_a p_0}. \quad (5)$$

Next, approximating infrared emission to space at a given frequency as coming from a narrow pressure range in the atmosphere, one can write an emission pressure corresponding to $\tau(p, \nu) = \tau_{\rm em}(\nu)$. Combining Equations (3) and (5), noting that τ and σ are proportional, setting $\tau_{\rm em} = 1$, rearranging in terms of ν, and writing $\nu = \nu_{\rm em}$ yields (Jeevanjee et al. 2021)

$$\nu_{\rm em}(p, x) = \nu_{\rm cen} \pm w \ln\left[\frac{x\sigma_{cen,0}p^2}{2g\overline{\mu} m_a p_0}\right]. \quad (6)$$

The logarithmic dependence of $\nu_{\rm em}$ on x is what gives rise to the logarithmic dependence of ΔF on x. The relationship between $\nu_{\rm em}$ and ΔF can be determined by noting that increasing x is equivalent to swapping emission over a certain frequency range from the surface to the stratosphere (Romps et al. 2022). The expression for the CO_2 radiative forcing parameter that emerges from this analysis is

$$\alpha = 2\pi w[\mathcal{B}(\nu_{\rm cen}, T_s) - \mathcal{B}(\nu_{\rm cen}, T_t)]. \quad (7)$$

Here, $\mathcal{B}(\nu, T)$ is the Planck spectral irradiance evaluated at frequency ν and temperature T, T_s is the surface temperature, and T_t is the tropopause temperature (see Figure 1).

The analytic model represented by Equation (7) is highly simplified, but it allows greater insight into the mechanism of CO_2 radiative forcing than is possible from numerical approaches. Like all current approaches to understanding climate change, however, it still requires us to assume that the infrared spectrum of CO_2 is available as a predetermined input. Our aim here is to relax this requirement, and derive w and $\nu_{\rm cen}$, and hence Equations (1) and (7), from the basic properties of the CO_2 molecule.

Table 1
Key Parameters Used in the Analysis

Parameter	Symbol	Value	Units
Mass of oxygen atom	$m_{\rm O}$	16	m_u
Mass of carbon atom	$m_{\rm C}$	12	m_u
Equilibrium C–O separation in CO_2	a_e	1.16×10^{-10}	m
CO_2 symmetric stretch force constant	k	1680	N m^{-1}
CO_2 bending mode force constant	k_δ/a_e^2	57	N m^{-1}
CO_2 transition dipole moment magnitude	$\lvert\langle m\rvert\boldsymbol{d}\lvert n\rangle\rvert$	3.35×10^{-31}	C m
CO_2 Fermi coupling term	$\lvert b\rvert$	2.14×10^{12}	Hz
Collision cross section (CO_2 in N_2)	σ_c	0.44×10^{-18}	m^2
Line-broadening coefficient	n_b	0.5	[]
Earth mean surface pressure	p_s	10^5	Pa
Earth mean surface temperature	T_s	288	K
Earth stratospheric temperature	T_t	217	K

Notes. Throughout this paper, we assume that reference pressure and temperature are equal to their surface values, $p_0 \equiv p_s$ and $T_0 \equiv T_s$. m_u is the atomic mass unit such that 1 $m_u = 1.66 \times 10^{-27}$ kg. Values for a_e, k, k_δ/a_e^2, and $|b|$ are taken from Herzberg (1945, pp. 21, 173, and 218); σ_c is from Chapman & Cowling (1990, p. 263). Values for other quantities are justified in the main text.

3. CO_2 Infrared Spectroscopy

CO_2 absorbs in the infrared due to combinations of vibrational and rotational quantum transitions (Pierrehumbert 2011). As a three-atom linear molecule, CO_2 has $3N - 5 = 4$ vibrational degrees of freedom (Figure 3), with four quantum numbers V_1, V_{2a}, V_{2b}, and V_3 corresponding to excitation of an symmetric stretch mode, two degenerate bending modes, and an asymmetric stretch mode, respectively.[7] Superposition of the in-plane and out-of-plane bending motions corresponding to V_{2a} and V_{2b} results in an excitation where the three atoms perform circular motions about the molecule's major axis (Figure 3). Such motion has angular momentum, which can be represented via introduction of a new quantum number l. Because V_{2a} and V_{2b} are degenerate, vibrational CO_2 states can therefore be characterized as $|V_1 V_2^l V_3\rangle$, where $V_2 = V_{2a} + V_{2b}$ and $l = V_2$,

[5] Traditionally, one of the novelties of atmospheric spectroscopy work is a continuous need to interconvert between various non-SI units. Here, we stick to SI units as much as possible, but when stating frequencies in hertz or terahertz we also report wavenumber values in centimeters, to allow easy comparison with other work.

[6] This is a simplified approach, because pressure scaling at line centers and line wings differs (Goody & Yung 1995; see also Section 3.2). However, the approach works well in practice (Romps et al. 2022), and the specific choice of pressure scaling in this equation does not affect our subsequent analysis.

[7] The use of ν as the symbol for frequency and v for vibrational quantum number is common in the modern spectroscopic literature, but to avoid confusion we have chosen to use the upper-case V notation of Adel & Dennison (1933) for quantum number here.

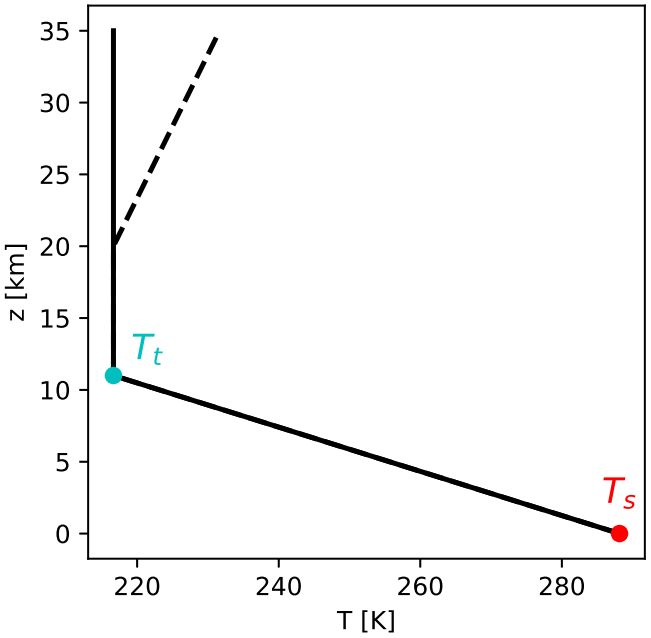

Figure 1. Idealized plot of temperature vs. altitude in Earth's atmosphere. The solid black line shows the temperature structure used to derive Equation (7) (fixed tropospheric lapse rate of $-6.5\,\mathrm{K\,km^1}$, isothermal stratospheric temperature of 217 K). The dashed black line shows the 1976 Standard Atmosphere temperature profile (Minzner 1977). Red and cyan dots show the values of T_s and T_t, respectively.

$V_2 - 2,\ldots,1$ or 0.[8] Hence, for $V_2 = 3$, for example, l can be 3 or 1, while for $V_2 = 4$, $l = 4$, 2, or 0 are all allowed.

The frequency of each vibrational mode of CO_2 can be calculated approximately by treating the molecule as three point masses connected by spring-like bonds.[9] In particular, using a valence force approach, which assumes restoring forces act to oppose changes in the distance and angles of local atom–atom bonds only (e.g., Herzberg 1945), the molecular vibrational potential energy U can be written as

$$U = U_e + \frac{1}{2}k(Q_1^2 + Q_2^2) + \frac{1}{2}k_\delta \delta^2. \tag{8}$$

Here, U_e is the equilibrium potential energy corresponding to zero vibrational motion, while Q_1 and Q_2 are the change in separation between the C and the first and second O atoms during vibrational motion, respectively. δ is the change in bond angle that occurs during bending motion, and k and k_δ are linear and bending bond force constants, respectively.

The form of the terms in Equation (8) allows the normal mode frequencies of the molecule to be simply expressed. We focus on the first two modes here. While the antisymmetric stretch mode ν_3 gives rise to a strong absorption band, it is located outside the thermal infrared spectral region and hence is not relevant to our discussion. Additional combination bands involving ν_3 are present around 30 THz ($1000\,\mathrm{cm^{-1}}$) but only contribute around 5% to radiative forcing at present-day CO_2 concentrations (Mlynczak et al. 2016).

For the symmetric stretch mode, we simply have oscillatory motion of each O atom, leading to

$$\nu_1 = \frac{1}{2\pi}\sqrt{\frac{k}{m_O}} \approx 40.1\ \mathrm{THz}\ (1337\,\mathrm{cm^{-1}}), \tag{9}$$

where m_O is the mass of an oxygen atom. The value $k = 1680\,\mathrm{N\,m^{-1}}$ yields $\nu_1 = 40.1$ THz ($1337\,\mathrm{cm^{-1}}$). This is fairly close to the C–O bond force constant of $1860\,\mathrm{N\,m^{-1}}$ in carbon monoxide (CO). The bending mode frequency is

$$\nu_2 = \frac{1}{2\pi}\sqrt{\frac{2}{m_O}\left(1 + 2\frac{m_O}{m_C}\right)\frac{k_\delta}{a_e^2}}, \tag{10}$$

where m_C is the mass of a carbon atom (Herzberg 1945). For $k_\delta = 7.7 \times 10^{-19}$ N m and $a_e = 116$ pm (Table 1), the value of ν_2 is 20.0 THz ($667\,\mathrm{cm^{-1}}$). ν_2 is of course the well-known bending mode associated with the center of the thermal infrared band, ν_{cen}, as seen in Figure 2. The fact that ν_2 is (apparently coincidentally) about half the value of ν_1 will be very important in the discussion that follows.

3.1. Line Positions

Now we have an expression for the spectral location of the ν_2 band in Figure 2, we can start to build up a description of the band structure. For this, we need to know what determines the location, shape, and intensity of all the most important spectral lines. We tackle this problem step by step, starting with line location. We focus on explaining the most abundant isotopologue of CO_2, $^{12}C^{16}O_2$, on the basis that the contribution of all other isotopologues to CO_2 radiative forcing is minor (Shine & Perry 2023).

In the infrared, spectral lines appear because absorption or emission of photons causes quantized changes in the vibrational and/or rotational state of molecules. The center of the ν_2 band at 20 THz ($667\,\mathrm{cm^{-1}}$) corresponds to a vibrational transition from the ground state $|00^00\rangle$ to the first excited bending mode with angular momentum number $l = 1$, $|01^10\rangle$.[10] The band has a strong central peak called the Q branch (Figure 2) due to purely vibrational transitions, and P and R branches at lower and higher frequencies, respectively, due to combinations of vibrational and rotational transitions. Solution of the time-independent Schrödinger equation in spherical coordinates (Levine 1975) shows that the location of P- and R-branch lines relative to ν_2 is given by

$$\nu_{J,J+1} = (E_{J+1} - E_J)/h = 2B(J+1). \tag{11}$$

Here, h is Planck's constant, $J = 0$, 1, 2, … is the rotational quantum number, E_J is the energy of rotational state J, and the rotational constant $B = h/8\pi^2 I$, with moment of inertia $I = 2m_O a_e^2$. In addition, a_e is the equilibrium C–O separation in CO_2 (Table 1). For lines in the Q branch, there is no change in J, while in the P and R branches, $\Delta J = \pm 1$. For $^{12}C^{16}O_2$, transitions involving odd values of J are missing, because of selection rules arising from the zero spin of the oxygen atoms (Levine 1975). Given that $a_e = 116$ pm, $B = h/16\pi^2 m_O a_e^2 = 11.7$ GHz ($0.39\,\mathrm{cm^{-1}}$), so the spacing between the P- and R-branch lines

[8] As always, the Dirac or bra-ket notation represents quantum states, such that $|\psi\rangle = \int d^3\boldsymbol{x}\psi(\boldsymbol{x})|\boldsymbol{x}\rangle$, and $\langle\psi|\phi\rangle = \int \psi(\boldsymbol{x})^*\phi(\boldsymbol{x})d^3\boldsymbol{x}$ when written in terms of position $\boldsymbol{x}$ and wave functions ψ and ϕ.

[9] More accurate determination of vibrational frequencies can be achieved via ab initio methods (e.g., Rodriguez-Garcia et al. 2007).

[10] We use the term "ν_2 band" here and elsewhere for simplicity, but, as will become clear soon, transitions involving additional vibrational modes are also important to the larger band structure.

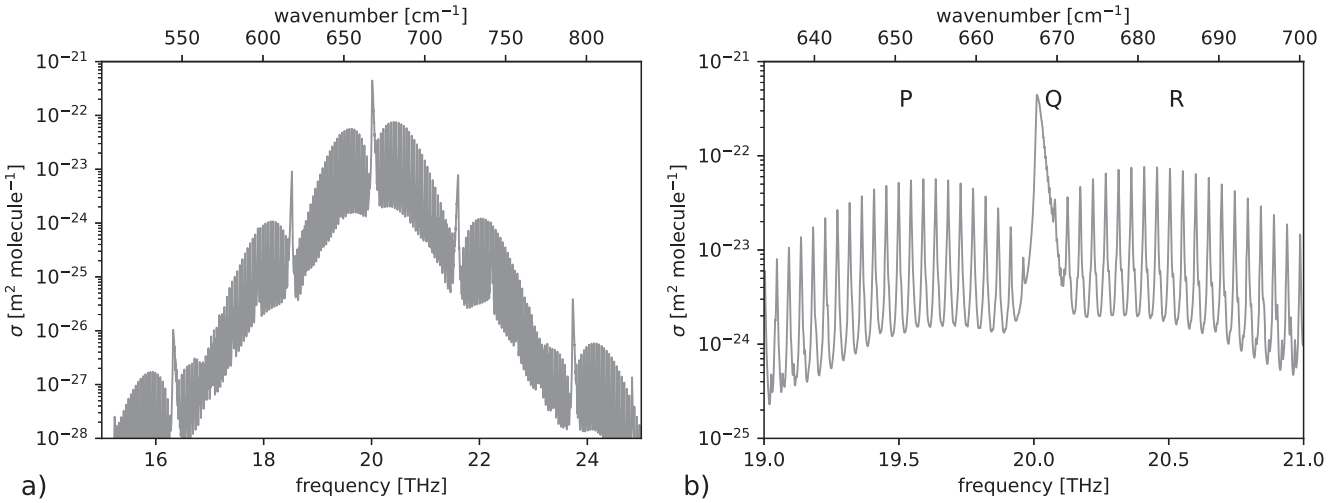

Figure 2. High-accuracy absorption spectrum of CO_2 in the region of the ν_2 band, in cross-section units of meters squared per molecule of CO_2, at pressure p_s and temperature T_s (see Table 1). (a) shows the band over a wide frequency range, while (b) zooms in on the central fundamental band, with P, Q, and R branches labeled (see Section 3). Both plots were produced using the HITRAN2020 database, with line truncation at the standard value of 25 cm^{-1}(0.75 THz) (Gordon et al. 2022).

is about $2 \times 2B = 47$ GHz (1.6 cm^{-1}). In the Q branch, transitions with different rotational energies are not exactly colocated because of subtle effects such as Coriolis interactions, but for our purposes the lines can be treated as unseparated in frequency. Rotational line spacing is further affected by centrifugal and anharmonic effects, but these complications are not important to climate forcing and so will be ignored here.

3.2. Line Shape and Width

All spectral lines have a shape that is determined by a combination of natural broadening, Doppler and collisional effects (Goody & Yung 1995). Line shape is dependent on both temperature and pressure. A full analysis of this problem could become complicated quickly, but in keeping with our aim of getting a rough estimate of CO_2 radiative forcing only, we take a simple approach here. In the troposphere, thermal infrared absorption lines are Lorentzian to a close approximation, with line shape

$$f(\nu - \nu_{mn}) = \frac{1}{\pi} \frac{\gamma}{(\nu - \nu_{mn})^2 + \gamma^2}, \tag{12}$$

where ν_{mn} is the frequency of the transition from state m to n and γ is the line width (half-width at half maximum) in hertz. γ scales approximately linearly with pressure. This can be shown by noting that the rms speed of a molecule in a gas of temperature T is

$$\bar{v} = \sqrt{3 k_B T / \overline{m}}, \tag{13}$$

where k_B is Boltzmann's constant, and $\overline{m}$ is the mean molecular mass of air. The mean relative collision speed is larger than this by a factor of $\sqrt{2}$, $\bar{v}_{rel} = \sqrt{2}\,\bar{v}$. The mean free path, or average distance traveled by a molecule between collisions, is (Chapman & Cowling 1990)

$$l_{mfp} = \frac{1}{\sqrt{2} n \sigma_c} = \frac{k_B T}{\sqrt{2}\,\sigma_c p}, \tag{14}$$

where σ_c is the intermolecular collision cross section, n is the number density, T is the temperature, p is the pressure, and $p = n k_B T$ from the ideal gas law. The line width in frequency units can be written as $\gamma = 1/(2\pi\tau_c) = \bar{v}_{rel}/(2\pi l_{mfp})$, where τ_c is the mean collision time between molecules.[11] Finally, we have

$$\gamma(p, T) = \gamma_0 (p/p_0)(T/T_0)^{-n_b}. \tag{15}$$

Here, $n_b = 0.5$, the reference values p_0 and T_0 are taken to be surface values (Table 1), and

$$\gamma_0 = \frac{\sigma_c p_0}{\pi} \sqrt{\frac{3}{\overline{m} k_B T_0}}. \tag{16}$$

For CO_2 in N_2, $\sigma_c = \pi \times (3.75 \times 10^{-10}\text{m})^2 = 0.44$ (nm)^2 (Chapman & Cowling 1990), so $\gamma_0 = 1.76$ GHz (0.06 cm^{-1}). The HITRAN2020 database (Gordon et al. 2022) gives values for γ_0 in the CO_2 ν_2 band that range between 1.5 and 3 GHz (0.05 cm^{-1} and 0.1 cm^{-1}), and n_b between 0.5 and 0.8, so our simple method slightly underestimates γ_0 and n_b. These differences are not important for the analysis that follows.

3.3. Line Intensity

Determining line intensity is one of the most challenging aspects of quantum spectroscopy. However, in the range of CO_2 concentrations over which radiative forcing scales approximately logarithmically according to Equation (1), ΔF is not sensitive to the absolute values of line intensity in the ν_2 band (e.g., Jeevanjee et al. 2021). Hence, we can also take an approximate approach here. The most important quantities in line intensity calculations are the Einstein coefficients, which express the rate of absorption or emission of a photon by a CO_2 molecule. Analysis of the Schrödinger equation in the presence of a time-dependent perturbation due to an oscillating electric field leads to the following expression for the Einstein

[11] The factor of 2π in the relationship between γ and τ_c can be obtained from a Fourier analysis of an ensemble of radiating oscillators (e.g., Stamnes et al. 2017).

coefficient for spontaneous emission:[12]

$$A_{mn} = \frac{16\pi^3\nu_{mn}^3|\langle m|\boldsymbol{d}|n\rangle|^2}{3hc^3\epsilon_0}. \quad (17)$$

Here, m and n are any two quantum states of energy E_m and E_n such that $E_m > E_n$ and $\nu_{mn} = (E_m - E_n)/h$. In addition, c is the speed of light and ϵ_0 is the vacuum permittivity. The term $\langle m|\boldsymbol{d}|n\rangle$ is the transition dipole moment, which is defined as

$$\langle m|\boldsymbol{d}|n\rangle \equiv \langle n|\boldsymbol{d}|m\rangle = \int \psi_m(\boldsymbol{x})^*\boldsymbol{d}\psi_n(\boldsymbol{x})d^3\boldsymbol{x}. \quad (18)$$

Here, $\boldsymbol{d}$ is the dipole moment operator of the molecule and ψ_k is the eigenfunction of quantum state k. The transition dipole moment has typical magnitude 3.34×10^{-31} C m (0.1 D) for CO_2 transitions in the ν_2 vibration-rotation band. This is similar to the permanent dipole of the ground state of CO, 4.07×10^{-31} C.m (0.122 D) (Muenter 1975). Taking $\nu_{mn} =$ 20 THz yields $A_{mn} \approx 1\ s^{-1}$. Comparison with HITRAN data shows that this is a reasonable approximation at the center of the ν_2 band, although the values of A_{mn} decrease away from the band center.

Line intensity expresses the frequency-integrated absorption cross section of a line, independent of line shape. In SI units of Hz m^2 $molecule^{-1}$, it is defined as[13]

$$S_{mn} = \frac{c^2A_{mn}}{8\pi\nu_{mn}^2}\mathcal{O}_{mn}(T). \quad (19)$$

The dimensionless term $\mathcal{O}_{mn}(T)$ incorporates multiple additional effects, of which the most important here is energy level occupancy. The rate of absorption of photons by molecules in a given energy state must depend on the number density of molecules in that state, relative to the total number density. At temperatures in the 250–290 K range, most CO_2 molecules are in the ν_2 vibrational ground state,[14] so the fundamental band vibrational occupancy factor can be approximated as 1 for our purposes. For the rotational state, however, occupancy up to J values of around 50 is significant at Earth-like temperatures. We take this into account by writing

$$\mathcal{O}_{mn}(T) = (2J + 1)e^{-J(J+1)hB/k_BT}/q_r, \quad (20)$$

with the rotational partition function approximated as $q_r \approx k_BT/2hB$ (Bernath 2020). The $(2J + 1)$ term in this expression accounts for degeneracy, i.e., for a given J value, there are $2J + 1$ states with the same energy.

The final step is to use line intensities to calculate the absorption spectrum itself. This is done by noting that the absorption cross section for a single line, in units of meters squared per molecule, is simply

$$\sigma_{mn} = S_{mn}f(\nu - \nu_{mn}), \quad (21)$$

and the total absorption cross section for the entire band is the sum of σ_{mn} over all transitions:

$$\sigma(\nu) = \sum_{mn}\sigma_{mn}. \quad (22)$$

Now we have all the pieces required to begin building absorption spectra. Using the line locations from Section 3.1, line shape and width definitions from Section 3.2, and line intensity formulae from this section, we can plot the P, Q, and R branches of the ν_2 fundamental band (Figure 4). Here, we have included lines up to $J = 100$, on the basis that lines from higher-rotational-number transitions are so weak that they contribute little further to absorption. Comparison with Figure 2 shows that line peaks are a little higher than in the HITRAN spectrum, mostly because we are somewhat underestimating the line-broadening coefficient γ via Equations (15) and (16). Otherwise, the overall form of the band center is reproduced fairly accurately. At the sides of the band, however, it is clear that our approach fails completely. Correctly incorporating these sidebands will be the task of the next section.

4. Fermi Resonance

The multiple sidebands present in the spectrum in Figure 2 arise due to vibrational transitions between higher-energy states than the $|00^00\rangle$ fundamental (Figure 5). In a perfect simple harmonic oscillator, the spacing of vibrational energy levels is uniform, and all transitions occur at the same frequency. This is clearly not the case for the CO_2 ν_2 band. The reason for the difference is Fermi resonance (Fermi 1931; Adel & Dennison 1933). Fermi resonance is far better known in quantum spectroscopy than in climate physics, but it is key to understanding CO_2 radiative forcing. Recently, Shine & Perry (2023) extracted individual bands from the HITRAN database for the purpose of numerical calculations of the radiative forcing and found that Fermi resonance contributes approximately half of the total forcing magnitude. Here, we begin by discussing the physical nature of Fermi resonance, and then show how incorporating it in our derivation allows us to write down a quantum analytic formula for CO_2 radiative forcing.

Fermi resonance occurs in CO_2 because $\nu_1 \approx 2\nu_2$: The symmetric stretch frequency happens to be very close in value to double the bending frequency. As a result, nonlinear interactions between the two modes shift the energy levels of states $|10^00\rangle$ and $|02^00\rangle$ and cause their wave functions to mix (Figure 5). The best way to get an intuitive understanding of Fermi resonance is by analogy with the classical coupled pendulum experiment. This analogy is noted in passing in Herzberg (1945), but we describe it in more detail here.

In the coupled pendulum experiment, two pendulums of almost equal natural frequencies exchange energy with each other via some nonlinear coupling (most commonly, torsion of the string to which they are attached). Without this nonlinear interaction, a Fourier transform of their motion would yield a single peak. However, when the pendulums are coupled, the same transform yields two peaks that are shifted from the original central value by an amount that depends on the strength of the interaction.

Mathematically, we can understand this process by first writing the classical Hamiltonian for a simple harmonic

[12] In many textbooks, the Einstein A coefficient is written in cgs units as $A_{mn} = 64\pi^4\nu_{mn}^3|\langle m|\boldsymbol{d}|n\rangle|^2/3hc^3$. To convert, note that in cgs units $\epsilon_0 = 1/4\pi$, which when substituted into the previous expression yields Equation (17).

[13] In HITRAN notation (Šimečková et al. 2006), we would write $\tilde{S}_{mn} = (A_{mn}/8\pi c\tilde{\nu}_{mn}^2)\mathcal{O}(T)$, where $\tilde{S}_{mn}$ has units of cm^{-1} (cm^{-2} $molecule$)$^{-1}$. To convert, we use $\tilde{\nu} = \nu/c$, and in addition $S_{mn} = c\tilde{S}_{mn}$.

[14] This can be seen by calculating the Boltzmann factor $e^{-h\nu_2/k_BT}$, which equals 0.036 given $T = 288$ K. This also indicates that neglecting stimulated emission is a good approximation in this case.

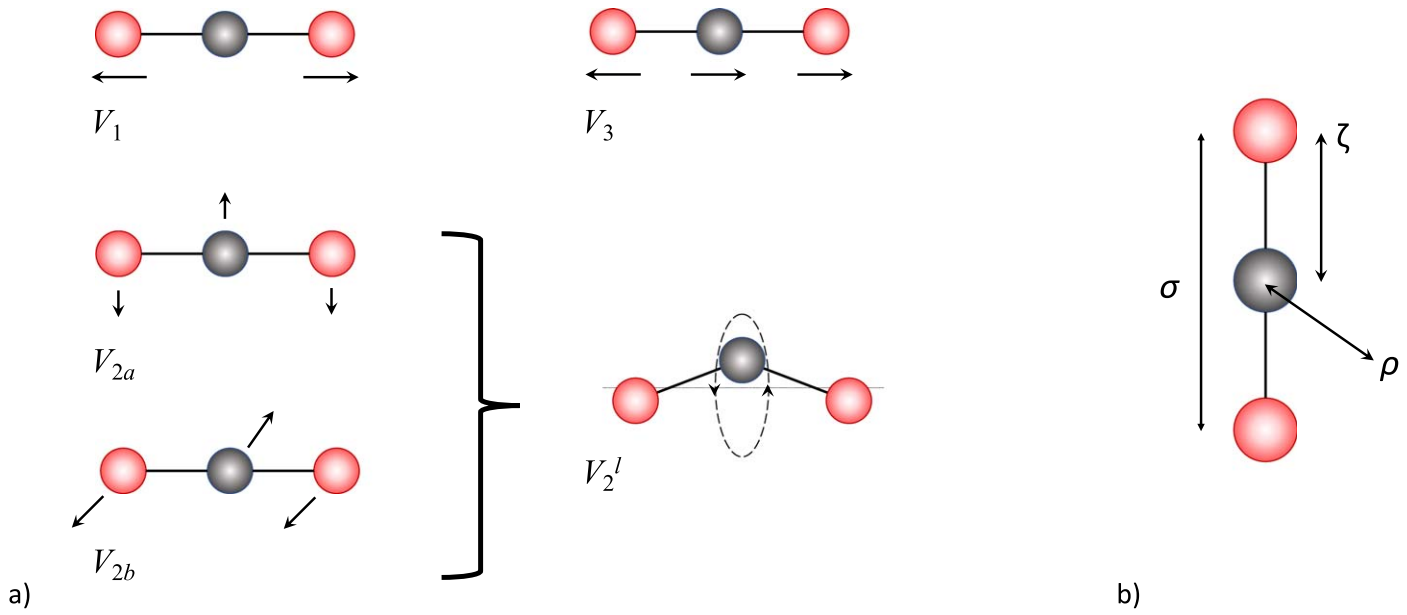

Figure 3. (a) Schematic of the three vibrational modes of carbon dioxide. The two degenerate bending modes superimpose to produce a motion where each atom rotates around the major axis of the molecule, which is represented via the quantum number l. (b) Mass-weighted coordinate system used to express the three fundamental modes of CO_2 as simple harmonic oscillations (see Section 4).

oscillator in isolation:

$$H(x, p) = \frac{1}{2}\frac{p^2}{m} + \frac{1}{2}kx^2. \tag{23}$$

Here, p is the momentum, m is the mass, k is a force constant, and x is the position. For two oscillators with a nonlinear coupling constant α, the Hamiltonian is

$$H(x_1, p_1, x_2, p_2) = \frac{1}{2}\frac{p_1^2}{m} + \frac{1}{2}\frac{p_2^2}{m} + \frac{1}{2}kx_1^2 + \frac{1}{2}kx_2^2 + \alpha x_1 x_2. \tag{24}$$

Using $d\boldsymbol{p}/dt = -\partial H/\partial \boldsymbol{x}$ and $d\boldsymbol{x}/dt = +\partial H/\partial \boldsymbol{p}$, where $\boldsymbol{x} = (x_1, x_2)$ and $\boldsymbol{p} = (p_1, p_2)$, we can derive equations of motion for each oscillator in the coupled case:

$$\frac{d^2x_1}{dt^2} = -\omega_0^2 x_1 - \tilde{\omega}^2 x_2, \tag{25}$$

$$\frac{d^2x_2}{dt^2} = -\omega_0^2 x_2 - \tilde{\omega}^2 x_1. \tag{26}$$

Here, $\omega_0 = \sqrt{k/m}$ and $\tilde{\omega} = \sqrt{\alpha/m}$. The coupling term $\tilde{\omega}$ causes energy to be repeatedly exchanged between the first and second oscillators (Figure 6). Taking the sum and difference of Equations (25) and (26) and writing $y_1 = x_1 + x_2$, $y_2 = x_1 - x_2$, we have

$$\frac{d^2y_1}{dt^2} = -\omega_+^2 y_1, \tag{27}$$

$$\frac{d^2y_2}{dt^2} = -\omega_-^2 y_2, \tag{28}$$

where $\omega_-^2 = \omega_0^2 - \tilde{\omega}^2$ and $\omega_+^2 = \omega_0^2 + \tilde{\omega}^2$. With this change of variables, it can be seen that the nonlinear coupling gives rise to two new eigenfunctions whose frequencies are shifted away from the unperturbed frequency ω_0 by an amount dependent on the coupling constant α. This is directly analogous to the way in which nonlinear coupling between the symmetric stretch and bending modes of CO_2 give rise to the Fermi bands. Figure 6 shows nondimensional numerical solutions of Equations (25) and (26) for $k = 2$, $m = 1$ and $\alpha = 0.1$, alongside the resulting power spectrum for x_1.

To represent Fermi resonance in a quantum framework, a degenerate first-order perturbation analysis can be used (Dennison 1940). For this, the molecular vibrational potential energy U discussed earlier is expressed in terms of dimensionless mass-weighted normal coordinates ζ, ρ, and σ (see Figure 3) and expanded as $U = U^0 + \epsilon U^1 + ...$, where ϵ is a perturbation parameter. This results in the expressions

$$U^0 = \frac{1}{2}h(\nu_1\sigma^2 + \nu_2\rho^2 + \nu_3\zeta^2), \tag{29}$$

$$\epsilon U^1 = \frac{1}{2}h(a\sigma^3 + b\sigma\rho^2 + c'\sigma\zeta^2). \tag{30}$$

Here, a, b, and c' have units of frequency. Equation (29) allows for simple harmonic oscillation of the CO_2 molecule at its three normal frequencies ν_1, ν_2, and ν_3, and nothing else. Equation (30) contains anharmonic terms, of which the second, $b\sigma\rho^2$, describes interaction between the bending and symmetric stretch modes. Because the potential energy must remain the same if the coordinates are reflected across a plane of symmetry of the molecule, all other cubic terms (ρ^3, ζ^3, etc.) in U^1 are forbidden for a linear molecule like CO_2.

With U defined, the Hamiltonian of the system is written in the form $H = H^0 + \epsilon H'$, and first-order degenerate perturbation theory (e.g., Robinett 2006) can be employed to derive a formula for the perturbed energy levels and wave functions. For clarity, we focus on the nearly degenerate states $|10^00\rangle$ and $|02^00\rangle$, which we assign wave functions ψ_m and ψ_n. Writing $\psi = a_m\psi_m + a_n\psi_n$, we can express the time-independent Schrödinger equation in the matrix form $\boldsymbol{Ha} = \boldsymbol{Ea}$, where the individual elements of $\boldsymbol{H}$ are $\langle\psi_i|H|\psi_j\rangle = \int\psi_i^* H\psi_j d^3\boldsymbol{x}$. With

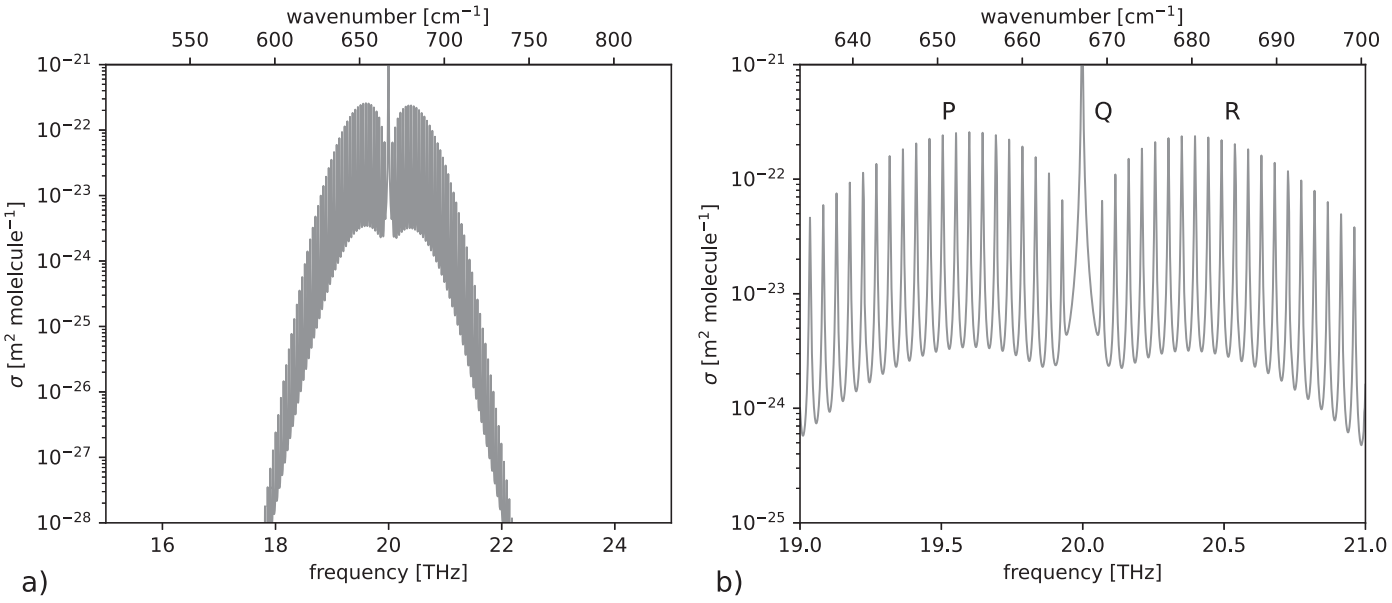

Figure 4. (a) Analytic CO_2 ν_2 band, including P, Q, and R branches for the fundamental vibrational transition from $|00^00\rangle$ to $|01^10\rangle$, but neglecting all additional vibrational transitions. (b) shows a close-up of the same band. Pressure and temperature are p_s and T_s in Table 1, as in Figure 2.

the expansion $H = H^0 + \epsilon H'$, we then have

$$\begin{pmatrix} E_m^0 + \epsilon W_{mm} & \epsilon W_{mn} \\ \epsilon W_{nm} & E_n^0 + \epsilon W_{nn} \end{pmatrix} \begin{pmatrix} a_m \\ a_n \end{pmatrix} = E \begin{pmatrix} a_m \\ a_n \end{pmatrix}, \tag{31}$$

where $W_{nm} = \langle \psi_n^0 | H' | \psi_m^0 \rangle$ and E_m^0 and E_n^0 are the unperturbed energies. Because of the symmetry of the system, $W_{mm} = W_{nn} = 0$ and $W_{nm} = W_{mn}^*$. Hence,

$$\begin{pmatrix} E_m^0 - E & \epsilon W_{mn} \\ \epsilon W_{mn}^* & E_n^0 - E \end{pmatrix} \begin{pmatrix} a_m \\ a_n \end{pmatrix} = 0. \tag{32}$$

Taking the determinant of the matrix to solve the eigenvalue equation, we have

$$(E_m^0 - E)(E_n^0 - E) - \epsilon^2 W_{mn}^* W_{mn} = 0. \tag{33}$$

Writing $(E_m^0 + E_n^0)/2 = \overline{E}^0$, setting $\epsilon = 1$, and solving for E yields

$$E_\pm = \overline{E}^0 \pm \frac{1}{2}\sqrt{(E_m^0 - E_n^0)^2 + 4|W_{mn}|^2}\,. \tag{34}$$

Explicit evaluation of the perturbation matrix element for states $|m\rangle = |10^00\rangle$ and $|n\rangle = |02^00\rangle$ (Adel & Dennison 1933; Herzberg 1945) yields the result that $|W_{10^00;02^00}| = hb/\sqrt{2}$. Writing the difference between state frequencies in the absence of resonance interaction as $\Delta_0 = (E_m^0 - E_n^0)/h$, we have the result that resonance makes two new states emerge with energy levels separated by $\Delta_F = \pm\sqrt{\Delta_0^2 + 2b^2}$. At the level of approximation we are using, the frequency difference $|\Delta_0| = 0.5$ THz (16.7 cm^{-1}), and the strength of coupling between the two modes $b = 2.14$ THz (71.3 cm^{-1}), so $\Delta_F = 3.07$ THz (102.3 cm^{-1}). Interestingly, these values of $|\Delta_0|$ and b were originally first determined from the spectra of CO_2 itself (both absorption and Raman; Fermi 1931; Dennison 1940).

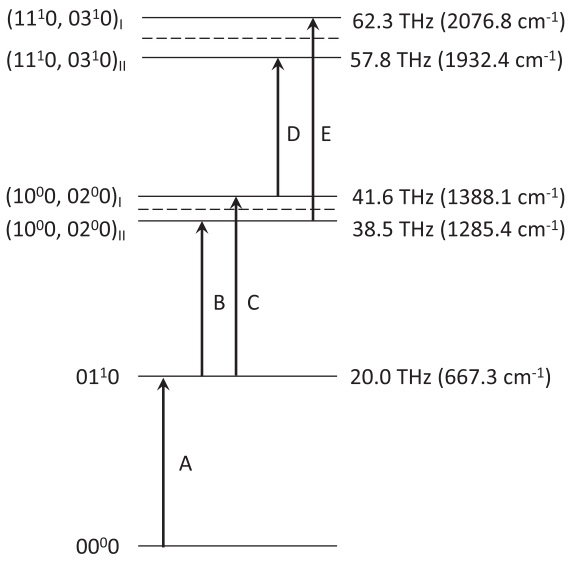

Figure 5. The key vibrational energy levels and transitions of the CO_2 molecule that are most important to radiative forcing and climate change. Many levels and transitions have been neglected for simplicity. Comparing with the notation of Shine & Perry (2023), our A ≡ Fu; B, C ≡F1; D, E ≡ FF; and H1, H2, and F2 are neglected. Numerical values for the energy levels were obtained from Oberly et al. (1968).

5. Radiative Forcing

Using the results of the previous two sections, we can now plot a revised synthetic spectrum for the CO_2 ν_2 band. The new Fermi resonance bands B and C (Figure 5) are modeled just like the fundamental band, with the difference that they are shifted to lower/higher frequencies by an amount $|\Delta_F|/2$, and to lower line intensities by addition of a vibrational occupancy factor to $\mathcal{O}_{mn}(T)$. We take this to be the ratio of occupancy of the ground states for each transition, or $e^{-h\nu_2/k_BT}$. We add the second set of Fermi bands D and E in a similar way, shifting them to lower/higher frequencies by a factor $|\Delta_F|$ and to lower line intensities by $e^{-2h\nu_2/k_BT}$. Recent analysis of radiative transfer model results shows that the fundamental band A

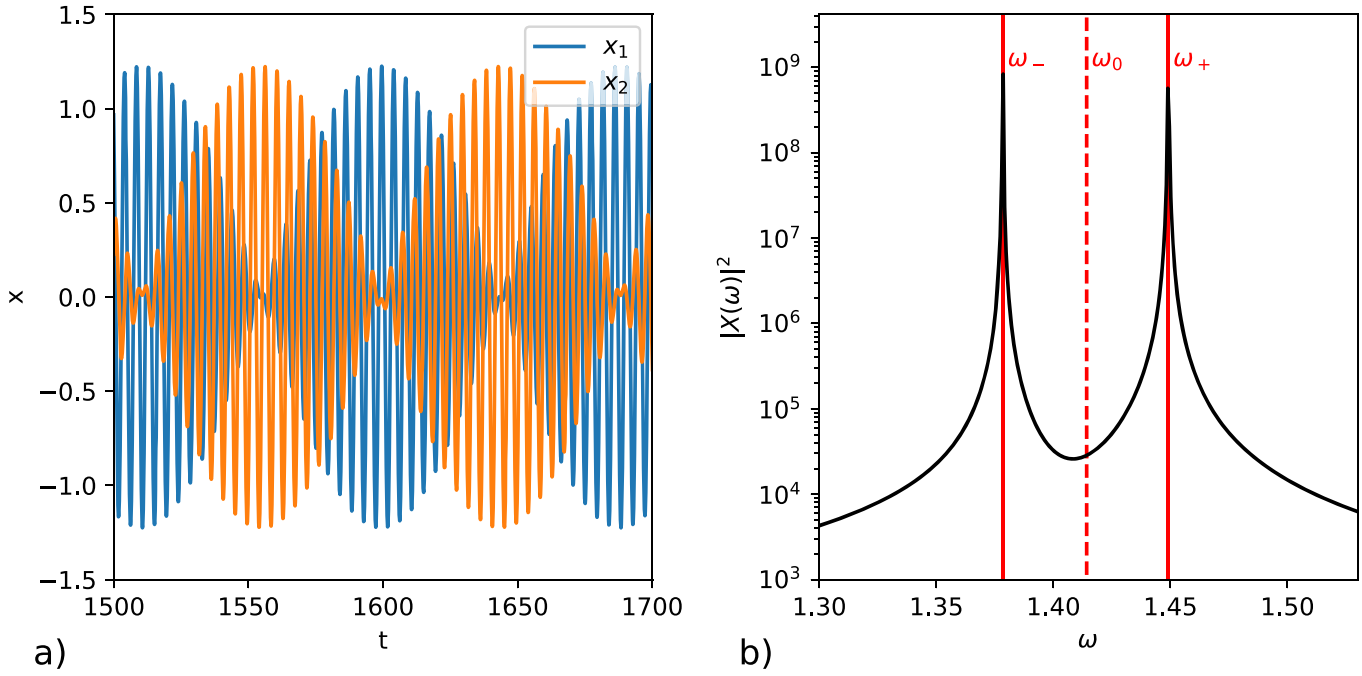

Figure 6. Classical analogy to Fermi resonance. (a) Numerical solution of Equations (25) and (26) and (b) the resulting power spectrum of x_1, with the analytical values of ω_0, ω_-, and ω_+ also shown. The simulation was run from $t = 0$ to $t = 10^4$ and solved using the 5(4)-order Runge–Kutta method. In the analogy, ω_0 is equivalent to ν_2 (times a factor of 2π), and ω_- and ω_+ are equivalent to the centers of the first Fermi sidebands.

contributes about 50% of CO_2 radiative forcing, while the additional Fermi bands B to E contribute most of the remaining 50% (Shine & Perry 2023). The contribution of other bands, such as the hot bands of the ν_2 fundamental and the "second Fermi" bands of Shine & Perry (2023), are neglected here on the basis that they do not cause sufficiently large changes in absorption in the spectral regions where they are present. Examples of such bands include the H1, H2, and F2 transitions mentioned in the caption to Figure 5.

As can be seen from Figure 7, inclusion of all the labeled transitions in Figure 5 results in a far more realistic mid-infrared absorption band for CO_2. Reference to Figure 2 shows that bands B and C are well captured by our approach. For bands D and E, the limitations of our simple methodology become more apparent, as they are both about 0.6 THz (20 cm^{-1}) too close to the fundamental band and too strong compared to HITRAN data. These differences arise due to our neglect of higher-order anharmonic terms, and our assumption of a constant value for the Einstein A coefficient.

Overall, however, inclusion of these four new Fermi bands results in a far more realistic mid-infrared absorption band for CO_2 than was shown in Figure 4. It is worth emphasizing that, despite the fact it reproduces the main P, Q, and R branches visible in the HITRAN CO_2 spectrum (Figure 2), the spectrum in Figure 4 is vastly simpler. The total number of lines in this spectrum is 750, whereas in the HITRAN CO_2 data set over the 15–25 THz (500–833 cm^{-1}) spectral range around 100,000 lines are present if all isotopologues are included. Many of these additional lines are not visible in Figure 2 because they are overlaid by the five strong bands incorporated in Figure 7.

We can also use the understanding developed in the last section to write down an analytic expression for the band structure coefficient w, and hence for CO_2 radiative forcing itself. Clearly, $\nu_{cen} = \nu_2$, and w must approximately equal half of $|\Delta_F|$ divided by the negative log of the occupancy factor:

$$w = \frac{|\Delta_F|}{2}\frac{k_B T}{h\nu_2}. \quad (35)$$

Given $T = 250$ K and $\nu_2 = 20$ THz, $w = 0.40$ THz (13.3 cm^{-1}). The equivalent value obtained by fitting a full HITRAN spectrum is remarkably close at 0.375 THz (12.5 cm^{-1}) (Romps et al. 2022).[15]

Our value for w yields $\alpha = 7.39$ W m^{-2} when substituted into Equation (7). This is somewhat larger than the 5.35 W m^{-2} value derived from comprehensive radiative transfer codes, or the slightly higher effective radiative forcing values derived from Earth-system models (Pinnock et al. 1995; Myhre et al. 1998; Masson-Delmotte et al. 2021).[16] The difference is primarily a result of the assumptions made in deriving Equation (7), and not our approach to calculating the CO_2 spectrum, as demonstrated by the close correspondence of our w value with that in Romps et al. (2022). Refinement of the derivation leading up to Equation (7) could be interesting to investigate in the future.

[15] Romps et al.'s (2022) *b*, which has a value of 0.04 cm, is equal to 1/2 times the inverse of our w expressed in centimeters.

[16] Technical note: There are different definitions of radiative forcing (e.g., Masson-Delmotte et al. 2021), which represents the perturbation to the planetary radiation budget due to a change in (in our case) of CO_2, in the absence of any surface-temperature change. The simplest definition is the "instantaneous radiative forcing" in which only CO_2 is changed. "Stratosphere-adjusted radiative forcing" allows stratospheric temperatures to adjust to the CO_2 perturbation; this is a better predictor of surface-temperature change, particularly when comparing the effect of changes in different constituents. IPCC's now-preferred definition ("effective radiative forcing") allows additional atmospheric adjustments (e.g., to tropospheric temperatures, humidity, and clouds); it is an even better predictor, although detailed Earth-system model calculations are needed to compute these adjustments. For the explanatory purposes of this paper, the differences between these definitions are of secondary importance.

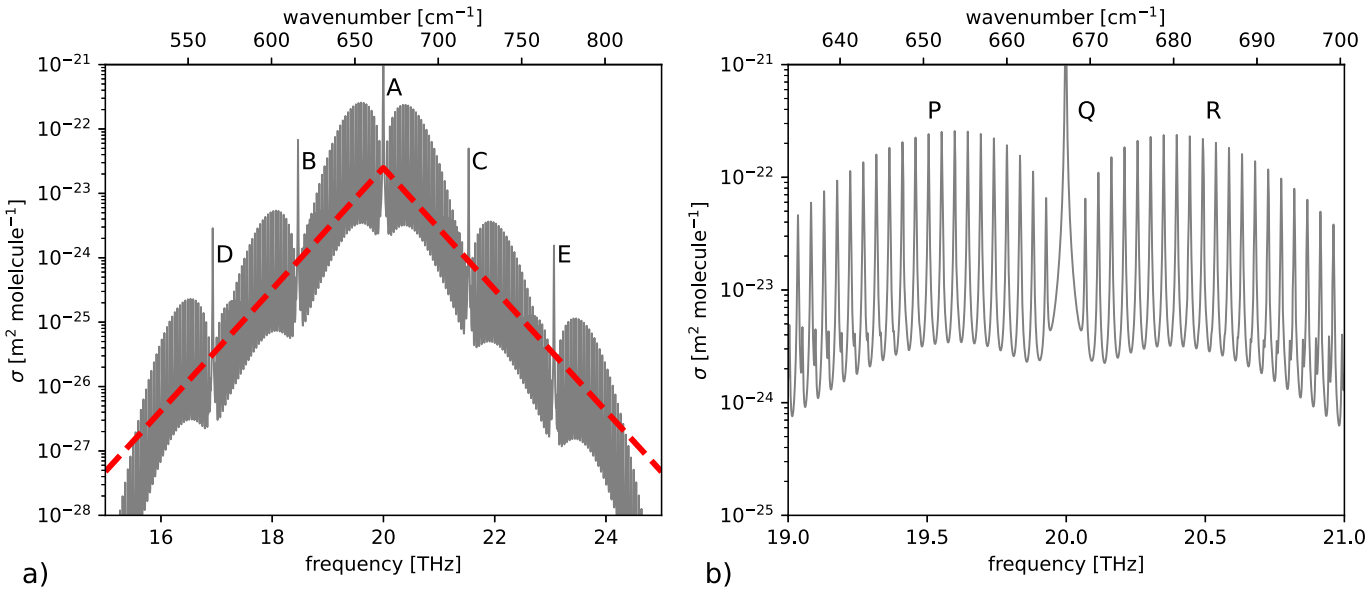

Figure 7. Analytic CO_2 ν_2 band, including the fundamental vibrational transition and four additional Fermi sidebands. The red line in panel (a) shows the approximate band shape predicted using Equations (3) and (35), given $T = T_s$. Labels in (a) correspond to the transitions in Figure 5. (b) shows a close-up of the fundamental band. Pressure and temperature are the same as in Figure 2.

Finally, we can use the result just obtained to write an approximate expression for the radiative forcing from CO_2 doubling as

$$\Delta F_{2\times} \approx \frac{\pi \ln(2) k_B T |\Delta_F|}{h\nu_2} \times [\mathcal{B}(\nu_2, T_s) - \mathcal{B}(\nu_2, T_t)] \approx 5.1 \text{ W m}^{-2}. \quad (36)$$

Interestingly, almost all the background theory required to derive Equation (36) has existed since the first numerical CO_2 radiative forcing calculations were performed in the 1960s. While this equation does not provide us with any truly new information, it does show us that the key driver of anthropogenic climate change can be expressed purely in terms of the measured properties of Earth's atmosphere and the fundamental properties of the CO_2 molecule, without the need for any numerical calculations.

6. Climate Sensitivity

The preceding analysis shows that the value of CO_2 radiative forcing can be understood in terms of the quantum properties of the CO_2 molecule, with the influence of Fermi resonance on the band structure coefficient w particularly critical. To tie this analysis back to Equation (2) in the Introduction (Section 1) and link global warming to radiative forcing, the last thing we need is an expression for the climate feedback parameter λ. Analytic approaches to this problem have been discussed in detail in other recent works (Ingram 2010; Jeevanjee et al. 2021a; Seeley & Jeevanjee 2021; Stevens & Kluft 2022; Jeevanjee 2023; Koll et al. 2023), so we only provide a very brief summary here, in the interests of completeness.

The simplest possible definition of λ occurs on an airless planet, where all thermal emission comes from the surface. If the planet is also a blackbody, we have

$$\lambda = \frac{dF}{dT_s} = 4\sigma T_s^3. \quad (37)$$

This yields $\lambda \approx 5.4$ W m^{-2} K^{-1} for $T_s = 288$ K. This gives us an upper limit on λ on Earth, because of course in many spectral regions the atmosphere is optically thick, and radiation to space occurs much higher, where air is colder and thermal emission is lower.

In-depth analysis in the papers cited above shows that, under present-day conditions, emission in the mid-infrared H_2O window region is the dominant contributor to λ, so Equation (37) can be approximated by

$$\lambda = \frac{d}{dT_s} \int_{\nu_A}^{\nu_B} \pi \mathcal{B}(\nu, T_s) d\nu, \quad (38)$$

where ν_A and ν_B are the frequency limits of the window region. Using the Wien approximation, this integral can be written as

$$\lambda \approx \frac{2\pi h^2 \nu_w^4 \Delta\nu_w}{k_B c^2 T^2} e^{-h\nu_w/k_B T}, \quad (39)$$

where $\nu_w = (\nu_A + \nu_B)/2$ and $\Delta\nu_w = \nu_B - \nu_A$.

Writing $\nu_A = 21$ THz (700 cm^{-1}) and $\nu_B = 36$ THz (1200 cm^{-1}), we obtain $\lambda = 2.3$ W m^{-2} K^{-1}, which is within the range for the clear-sky long-wave feedback from observations and complex climate models (Andrews et al. 2012; McKim et al. 2021; Roemer et al. 2023).[17] Combining this estimate with the value for $\Delta F_{2\times}$ calculated in the last section yields $\Delta T_s = 2.2$ K. This is also reasonably close to values calculated using much more complicated models, despite the approximate nature of the calculation. As mentioned in the Introduction (Section 1), the range of modern estimates for ΔT_s extends to

[17] We leave the derivation of ν_A and ν_B from the quantum-mechanical properties of the H_2O molecule to future work.

higher values (2–5 K), in part because cloud feedbacks are predicted to increase warming in the future.

7. Discussion

We have shown using mostly first-principles reasoning how the radiative forcing of CO_2 emerges from the quantum-mechanical properties of the CO_2 molecule. This result has implications for our understanding of both contemporary global warming and the long-term evolution of Earth's climate. There are, of course, many things that our analysis misses out. Many spectroscopic details, including anharmonic interactions, line mixing, and additional weak bands have been neglected, as have overlap with other gaseous absorbers and the radiative effects of clouds. In common with many other 1D calculations, atmospheric vertical temperature structure has been treated crudely, and 3D dynamics is neglected entirely. Given all this, it is remarkable that our analysis and others like it still allows a reasonably accurate estimate of clear-sky radiative forcing and climate sensitivity. This outcome provides further evidence, if such evidence were needed, of the rock-solid foundation of the physics of global warming and climate change.

The work presented here should not be seen as a substitute for accurate numerical calculations, but instead a way to understand the fundamental physics that underpins them. As our approach to spectroscopy in this paper is rather specific to the problem at hand, it is not immediately clear if there are many future applications for doing calculations from first principles in this way. Nonetheless, it would be interesting to see if our approach could be extended to CO_2 radiative forcing on other solar system planets. Mars is likely to be an easier case than Venus in the solar system, because of the importance of CO_2 collision-induced absorption (CIA) in Venus's thick atmosphere, although in principle a simplified approach to CIA along the lines we have pursued here should also be possible.

Another interesting extension could be to use the analysis in Section 3 to provide quick estimates of the warming potential of different greenhouse gases in a planetary context. For exoplanet and paleoclimate applications, this might be a particularly useful way of increasing intuition and providing a reality check on the results of complex climate models. It might also be interesting to investigate in more detail why resonances appear in certain molecules and bands but not in others.

Finally, carbon dioxide has likely been a key greenhouse gas throughout Earth's history. Given this, the dependence of CO_2 radiative forcing on the accidental resonance between ν_1 and ν_2 is particularly interesting. One can imagine that with minor differences in the quantum structure of CO_2, this resonance might be changed or inhibited, and the past and future evolution of our planet's climate would be very different. In this sense, the CO_2 Fermi resonance may be seen as somewhat analogous to the nuclear resonances in astrophysics that give rise to the production of heavy elements in stellar interiors (Hoyle 1954; Livio et al. 1989).

Acknowledgments

We thank the organizers of the PCTS 2022 "From Spectroscopy to Climate: Radiative Constraints on the General Circulation" workshop for thought-provoking discussions that helped to motivate this article. We also thank Nadir Jeevanjee and an anonymous reviewer for insightful comments that significantly improved the quality of this manuscript. R.W. acknowledges additional discussions with Iouli Gordon on HITRAN unit conversion and related topics. R.W. and J.S. acknowledge funding from NSF awards AST-1847120 (CAREER) and AGS-2210757. Code to reproduce the plots in the paper is available open-source on GitHub with a copy deposited to Zenodo doi:10.5281/zenodo.10557939.

ORCID iDs

R. Wordsworth https://orcid.org/0000-0003-1127-8334

References

Adel, A., & Dennison, D. M. 1933, PhRv, 43, 716
Andrews, T., Gregory, J. M., Webb, M. J., & Taylor, K. E. 2012, GeoRL, 39, L09712
Bernath, P. F. 2020, Spectra of Atoms and Molecules (Oxford: Oxford Univ. Press)
Chapman, S., & Cowling, T. G. 1990, The Mathematical Theory of Non-uniform Gases: An Account of the Kinetic Theory of Viscosity, Thermal Conduction and Diffusion in Gases (Cambridge: Cambridge Univ. Press)
Dennison, D. M. 1940, RvMP, 12, 175
Dufresne, J.-L., Eymet, V., Crevoisier, C., & Grandpeix, J.-Y. 2020, JCli, 33, 3827
Fermi, E. 1931, ZPhy, 71, 250
Friedlingstein, P., Jones, M. W., O'Sullivan, M., et al. 2022, ESSD, 14, 1917
Goody, R. M., & Yung, Y. L. 1995, Atmospheric Radiation: Theoretical Basis (Oxford: Oxford Univ. Press)
Gordon, I. E., Rothman, L. S., Hargreaves, R. J., et al. 2022, JQSRT, 277, 107949
Herzberg, G. 1945, Molecular Spectra and Molecular Structure, Vol. 2: Infrared and Raman Spectra of Polyatomic Molecules (New York: Van Nostrand)
Hoyle, F. 1954, ApJS, 1, 121
Ingram, W. 2010, QJRMS, 136, 30
Jeevanjee, N., Koll, D. D. B., & Lutsko, N. J. 2021a, GeoRL, 48, e2021GL093699
Jeevanjee, N., Seeley, J. T., Paynter, D., & Fueglistaler, S. 2021, b, JCli, 34, 9463
Jeevanjee, N. 2023, AmJPh, 91, 731
Koll, D. D. B., Jeevanjee, N., & Lutsko, N. J. 2023, JAtS, 80, 1923
Levine, I. N. 1975, Molecular Spectroscopy (New York: John Wiley & Sons)
Livio, M., Hollowell, D., Weiss, A., & Truran, J. W. 1989, Natur, 340, 281
Masson-Delmotte, V., Zhai, P., Pirani, A., et al. 2021, The Physical Science Basis. Contribution of Working Group I to the Sixth Assessment Report of the Intergovernmental Panel on Climate Change (Cambridge: Cambridge Univ. Press),
McKim, B. A., Jeevanjee, N., & Vallis, G. K. 2021, GeoRL, 48, e94074
Minzner, R. A. 1977, RvGeo, 15, 375
Mlynczak, M. G., Daniels, T. S., Kratz, D. P., et al. 2016, GeoRL, 43, 5318
Muenter, J. S. 1975, JMoSp, 55, 490
Myhre, G., Highwood, E. J., Shine, K. P., & Stordal, F. 1998, GeoRL, 25, 2715
Oberly, R., Rao, K. N., Hahn, Y. H., & McCubbin, T. K., Jr 1968, JMoSp, 25, 138
Pierrehumbert, R. T. 2011, Principles of Planetary Climate (Cambridge: Cambridge Univ. Press),
Pinnock, S., Hurley, M. D., Shine, K. P., Wallington, T. J., & Smyth, T. J. 1995, JGR, 100, 23,227
Robinett, R. 2006, Quantum Mechanics: Classical Results, Modern Systems, and Visualized Examples (Oxford: Oxford Univ. Press)
Rodriguez-Garcia, V., Hirata, S., Yagi, K., et al. 2007, JChPh, 126, 124303
Roemer, F. E., Buehler, S. A., Brath, M., Kluft, L., & John, V. O. 2023, NatGe, 16, 416
Romps, D. M., Seeley, J. T., & Edman, J. P. 2022, JCli, 35, 4027
Seeley, J. T., & Jeevanjee, N. 2021, GeoRL, 48, e89609
Shine, K., & Perry, G. 2023, QJRMS, 149, 1856
Stamnes, K., Thomas, G. E., & Stamnes, J. J. 2017, Radiative Transfer in the Atmosphere and Ocean (2nd ed.; Cambridge: Cambridge Univ. Press),
Stevens, B., & Kluft, L. 2022, EGUsphere, doi:10.5194/egusphere-2022-1460
Šimečková, M., Jacquemart, D., Rothman, L. S., Gamache, R. R., & Goldman, A. 2006, JQSRT, 98, 130
Tziperman, E. 2022, Global Warming Science: A Quantitative Introduction to Climate Change and Its Consequences (Princeton, NJ: Princeton Univ. Press)
Wilson, D. J., & Gea-Banacloche, J. 2012, AmJPh, 80, 306
Zhong, W., & Haigh, J. D. 2013, Wthr, 68, 100